R 707

Technical Report

ULTIMATE HORIZONTAL SHEAR STRENGTH OF PRESTRESSED SPLIT BEAMS

January 1971

Sponsored by

NAVAL FACILITIES ENGINEERING COMMAND

NAVAL CIVIL ENGINEERING LABORATORY

Port Hueneme, California

47

ULTIMATE HORIZONTAL SHEAR STRENGTH OF PRESTRESSED SPLIT BEAMS

Technical Report R-707

YF 38.534.001.01.009

by

S. B. Nosseir and R. N. Murtha

ABSTRACT

This report deals with the horizontal shear resistance and behavior of prestressed concrete composite beams when the interface is selected to pass through the centroid of the composite section. Composite beams proportioned in this manner are referred to as prestressed split beams. A total of eight simply supported split beams were statically tested with the major variables being interface roughness and reinforcement parameter $r f_y$. (r and f_y are the percent and yield point of the web reinforcement across the interface.) All test beams were posttensioned and grouted and had the same nominal dimensions. Beams with rough interfaces showed an increase in the ultimate horizontal shear strength of about 100 psi over that of "duplicate" beams with smooth interfaces. The ductility and the energy absorption capacity increased with $r f_y$. The ultimate horizontal shear strength for beams with $r f_y = 0$ was in excess of 400 psi and increased at the rate of about 60 psi per 100 psi increase in $r f_y$. The two beams with the highest value of $r f_y$ failed in flexure. In spite of developing slip at the interface, these two beams developed the calculated flexural resistance based on full composite action. The horizontal shear resistance of the test beams failing in horizontal shear was much higher than the computed values based on the ACI code.

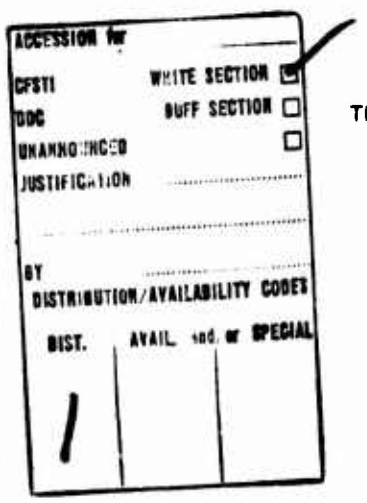

CONTENTS

INTRODUCTION

General

In order to minimize the amount of prestressing steel in a concrete beam, Amirikian[1] proposed that the prestressing be limited only to the zone which would be subject to tensile stresses if the beam were unprestressed. He termed this design criterion *split-beam prestressing*. A beam designed to satisfy this criterion may be thought of as a special case of a prestressed composite beam for which the interface is selected to pass through the centroid of the composite section.

Bryson and others[2] studied the flexural behavior of concrete beams prestressed according to Amirikian's proposed criterion; these beams were referred to as *prestressed split beams*, or simply, split beams. Their test results indicated that the ultimate resistance of split beams was very close to that of conventionally prestressed beams. They concluded that the adoption of the method of split-beam prestressing allows a significant reduction in the amount of prestressing steel. However, a detailed study of horizontal shear resistance of split beams was outside the scope of their investigation.

The possibility of horizontal shear failure of general composite beams has been of concern to many investigators.[3-8] Recommendations aimed at avoiding this type of failure can be found in many other publications,[9-15] but a general theory or even a hypothesis of failure that is consistent with the accepted theories of concrete failure is still nonexistent. The issue of finding a general expression for the horizontal shear resistance remains controversial.[16-20]

Since split beams are a special case of composite beams for which the maximum horizontal shear stresses occur at the interface, a study of the horizontal shear resistance of split beams is essential to ensure their "safe" design. Such a study could also shed more light on the behavior of general composite beams.

Objective

The overall objective of this study was to evaluate the horizontal shear strength at the interface between the precast and the cast-in-situ parts of a prestressed concrete split beam. Specifically, two objectives were

considered: (1) the influence of interface roughness on the horizontal shear strength, and (2) the effect of varying the amount and strength of the web steel across the interface on the behavior and shear-transfer strength of split beams.

Scope

Eight prestressed concrete split beams were statically loaded to failure. The eight test beams formed four sets, with each set composed of two beams that were "identical" except for the interface roughness. Interfaces were finished either to a rough surface using a wire brush or to a smooth surface using a steel trowel. The main variable among the four sets was the reinforcement parameter $\mathbf{r}\,\mathbf{f_y}$, where $\mathbf{r}$ is the percent of web reinforcement across the interface and $\mathbf{f_y}$ is the yield point of the web reinforcement. No attempt was made to vary the concrete strength, the level of prestressing, or the shear-span-to-depth ratio.

TEST PROGRAM

Test Beams

The test specimens consisted of eight posttensioned, prestressed composite (concrete-to-concrete) beams. Each beam was symmetrically loaded and simply supported over a span of 8 feet. The eight test beams constituted four pairs of companion specimens. The two beams of each pair were nominally identical, the only variable being the treatment (smooth or rough) of the interface between the precast and the cast-in-situ parts of the beam. The principal variable among the four pairs was the percent of web reinforcement *crossing* the interface.

In order to meet the conditions of split-beam prestressing,[1] the beam dimensions (Figure 1) were selected such that the interface would be at the same location as the centroidal axis of the composite section. The beams were also designed in such a way that high shear stresses would be produced at the interface prior to flexure, diagonal tension, or web failure.

The beams are designated by one letter followed by one number. The letter refers to the smooth (S) or rough (R) condition at the interface. The number is the value of the percent of reinforcement crossing the interface to the nearest 0.1%. For example, a beam designated by S0.7 has a smooth interface and a reinforcement crossing the interface of approximately 0.7%. Table 1 lists the properties of the test beams including the prestressing data.

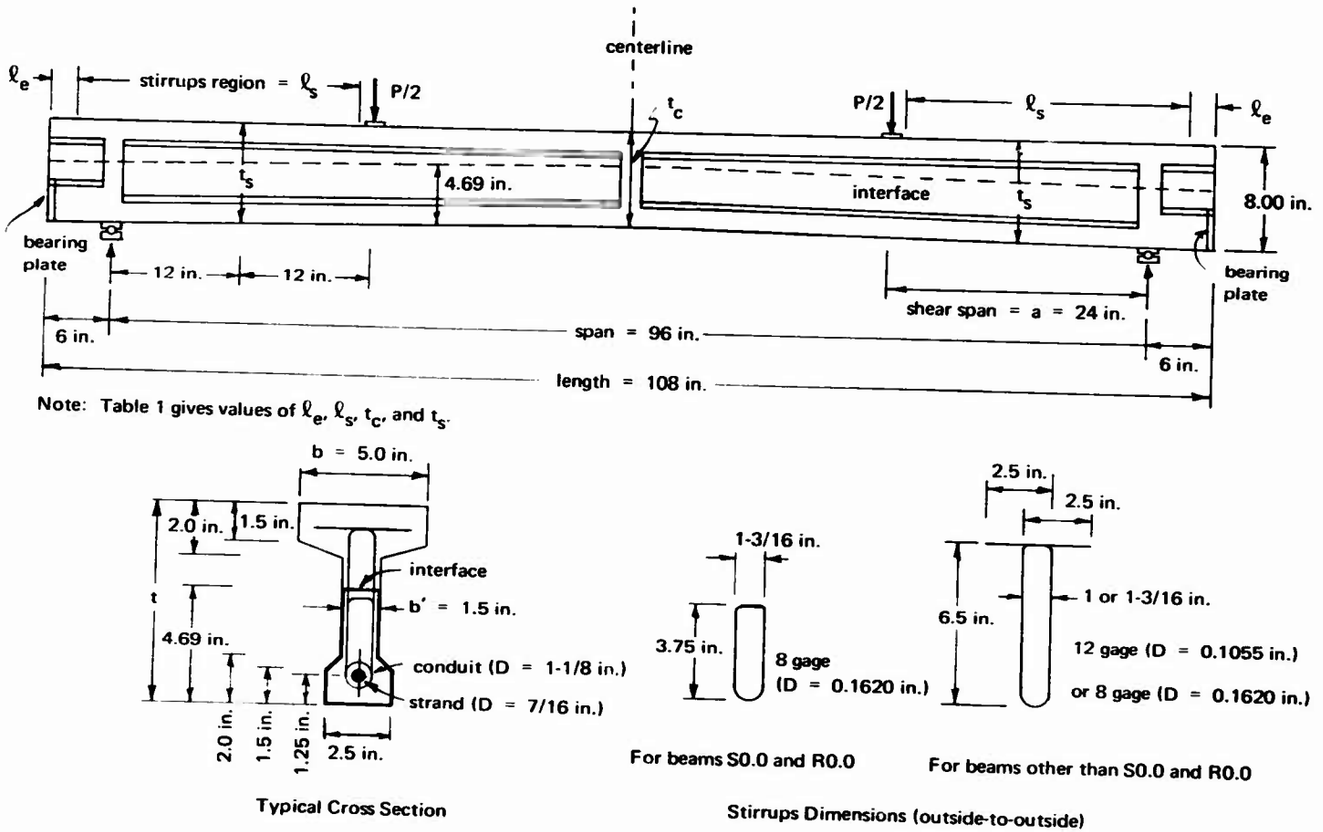

Figure 1. Details of test beams.

Table 1. Properties of Test Beams[a]

Beam Designation	Condition at Interface	t_c (in.)	t_s (in.)	d_c (in.)	d_s (in.)	$\frac{a}{d_s}$	p (%)	Stirrups Data								Prestressing Data					
																Forces (kips)			Stresses (ksi)		
								ℓ_e (in.)	ℓ_s (in.)	D (in.)	s (in.)	r_1 (%)	r (%)	f_y (ksi)	$r f_y$ (psi)	F_{sj}	F_{si}	F_{se}	f_{sj}	f_{si}	f_{se}
S0.0	smooth	7.5	7.75	6.25	6.5	3.69	0.349	2.00	26.0	0.1620	3-1/4	0.845	0	33.5	0	10.9	9.15	8.29	100	83.9	76.1
R0.0	rough	7.31	7.65	6.06	6.4	3.75	0.360	2.00	26.0	0.1620	3-1/4	0.845	0	33.5	0	13.0	9.35	8.37	119	85.8	76.8
S0.3	smooth	7.54	7.77	6.29	6.52	3.68	0.347	1.69	27.1	0.1055	3-7/8	0.299	0.299	24.6	73.5	11.8	9.18	8.42	108	84.2	77.2
R0.3	rough	7.31	7.66	6.06	6.41	3.74	0.360	1.69	27.1	0.1055	3-7/8	0.299	0.299	24.6	73.5	12.2	10.4	9.18	112	95.4	84.2
S0.7	smooth	7.56	7.78	6.31	6.53	3.68	0.345	0.75	28.2	0.1055	1-5/8	0.714	0.714	24.6	176	12.2	9.87	9.22	112	90.6	84.6
R0.7	rough	7.5	7.75	6.25	6.5	3.69	0.349	0.75	28.2	0.1055	1-5/8	0.714	0.714	24.6	176	11.5	7.81	6.54	106	71.7	60.0
S2.0	smooth	7.75	7.88	6.5	6.63	3.62	0.335	0.44	28.9	0.1620	1-3/8	2.000	2.000	33.5	670	13.8	10.3	9.53	127	94.5	87.4
R2.0	rough	7.75	7.88	6.5	6.63	3.62	0.335	0.44	28.9	0.1620	1-3/8	2.000	2.000	33.5	670	12.8	10.9	10.6	117	100	97.2

[a] See List of Symbols for definitions.

Materials

Concrete. Due to the small size of the beams, model concrete was used with the mix design based on the recommendations given in Reference 21. The concrete was a mixture of type III portland cement, San Gabriel River aggregate, and Port Hueneme city water. A cumulative gradation curve for the aggregate is shown in Figure 2. The concrete properties for all the beams are listed in Table 2, including concrete strengths obtained from tests of 6 x 12-inch control cylinders.

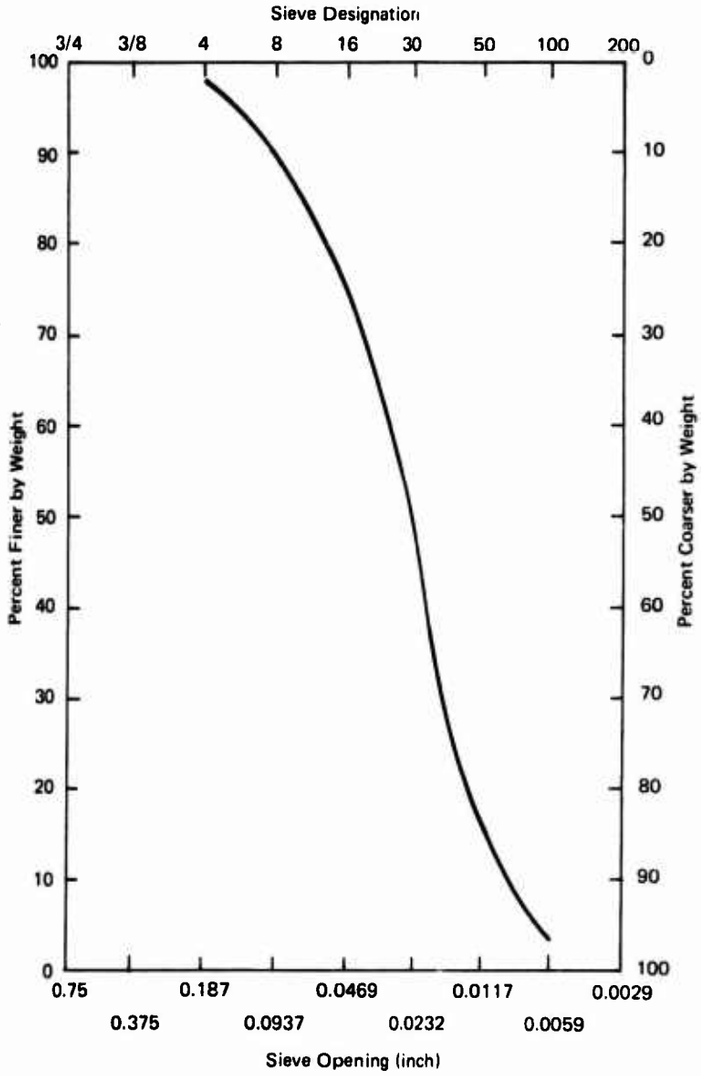

Figure 2. Sieve analysis of aggregate.

Table 2. Properties of Concrete

Beam Designation	Beam Section	Aggregate-to-Cement Ratio[a]	Water-to-Cement Ratio	Cement (sacks/yd^3)	Water (gal/sack)	Slump (in.)	Concrete Strength (psi)				Age (days)	
							f'_c		f_{sp}			
							P[b]	T[c]	P[b]	T[c]	P[b]	T[c]
S0.0	cast-in-situ	3.00	0.57	9.12	6.44	2.25	–	3,730	–	398	–	6
	precast	2.99	0.61	9.06	6.89	4	4,013	4,360	363	512	14	20
R0.0	cast-in-situ	3.00	0.58	9.09	6.62	2.75	–	3,747	–	390	–	6
	precast	3.00	0.59	9.07	6.73	4.75	3,748	4,483	413	470	10	17
S0.3	cast-in-situ	2.99	0.61	9.06	6.88	4.75	–	3,577	–	423	–	8
	precast	3.00	0.58	9.10	6.55	5	3,366	5,073	390	479	5	14
R0.3	cast-in-situ	3.00	0.60	9.06	6.78	3.5	–	3,340	–	418	–	8
	precast	2.99	0.58	9.12	6.54	5	3,233	4,603	–	500	6	14
S0.7	cast-in-situ	3.00	0.59	9.08	6.66	2.25	–	4,300	–	450	–	7
	precast	3.00	0.61	9.05	6.87	3	3,970	4,940	443	465	10	17
R0.7	cast-in-situ	3.00	0.61	9.04	6.88	2	–	3,987	–	433	–	7
	precast	3.00	0.55	9.16	6.26	4.25	3,830	4,893	423	457	9	16
S2.0	cast-in-situ	3.00	0.60	9.05	6.85	2.25	–	3,855	–	405	–	6
	precast	3.00	0.61	9.05	6.87	3	4,818	5,740	405	463	8	14
R2.0	cast-in-situ	3.00	0.56	9.14	6.31	5	–	3,748	–	410	–	6
	precast	3.00	0.63	9.00	7.14	2.5	4,638	5,294	453	405	8	14

[a] Weight of aggregate is in the saturated surface-dry condition with an absorption capacity of 1%.

[b] At the time of beam prestressing.

[c] At the time of beam testing.

Grout. The constituents of grout were extra fine aggregate (all passing U. S. standard sieve no. 100), cement (type III portland), water, and a water-reducing admixture (Plastocrete). The weight ratios of the aggregate to cement and the water to cement were 0.34 and 0.50, respectively. Plastocrete was added at the rate of about 5 ounces per 100 pounds of cement. Figure 3 shows the variation of grout strength with age for a trial batch with a water-to-cement ratio of 0.55 (by weight).

Reinforcing Steel. The prestressing steel used was seven-wire uncoated, stress-relieved strands, 7/16 inch in diameter and 0.109 $in.^2$ in area. Tests gave an average elastic modulus of 29×10^6 psi and an average ultimate stress of 243 ksi. A typical stress–strain curve is shown in Figure 4. The unstraightened strands were received in a coil about 5 feet in diameter, weighing about 200 pounds.

The web reinforcement was either 12-gage or 8-gage wires with a nominal diameter of 0.1055 inch or 0.162 inch, respectively. The yield point and ultimate stress averaged 24.6 ksi and 41.8 ksi, respectively, for the 12-gage wire; the corresponding values for the 8-gage wire were 33.5 ksi and 47.9 ksi. The stress–strain curves were of the type which have a long plateau at the yield point.

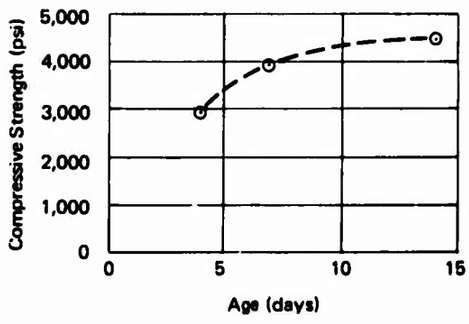

Figure 3. Variation of grout strength with age for 3 x 6-inch cylinders.

Fabrication

Forms. The test beam was cast in a steel and wood form. The steel section, which consisted of two 4 x 1-5/8-inch nominal-size channels connected to a 1/4-inch plate, was used in conjunction with two different wooden sections for casting both the precast and the cast-in-situ parts of the beam (Figure 5). The wooden section used for casting the cast-in-situ part was made in such a way that the camber of the precast part due to prestressing would be allowed without any restraint. The beam forms as well as the 6 x 12-inch control-cylinder molds were cleaned and oiled prior to each casting operation.

Mixing and Casting. All concrete was mixed in a 6-ft^3-capacity mixer with a nontilting drum. Before each batching, the moisture content for the aggregate was determined, and the weights of the ingredients were based on the saturated surface-dry condition of the aggregate. The mixing time was

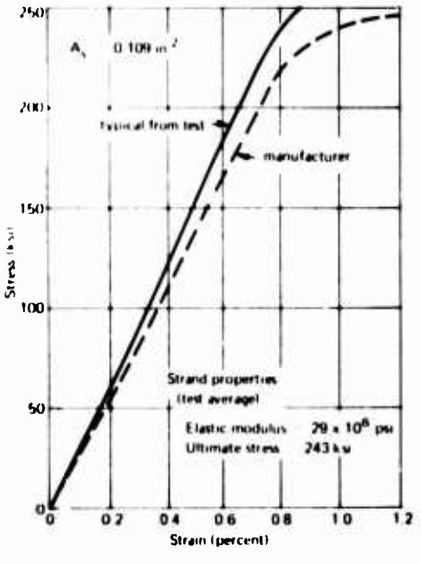

Figure 4. Tensile stress–strain curves for 7/16-inch seven-wire strand.

approximately 6 minutes. Following a butter mix of about 1 ft^3, a batch of about 4 ft^3 was used for each cast. Slump (Table 2) was measured immediately after mixing.

Twelve 6 x 12-inch control cylinders were cast with each precast part of the test beams, and six such cylinders were cast with each cast-in-situ part. Two high-frequency form vibrators provided continuous vibration of the beam form during casting. The concrete for each control cylinder was placed in two lifts; an internal vibrator was used for vibrating each lift.

Finishing and Curing. Several hours after casting, the concrete top surface of the precast beam part, that is, the interface, was finished to either a smooth surface using a steel trowel

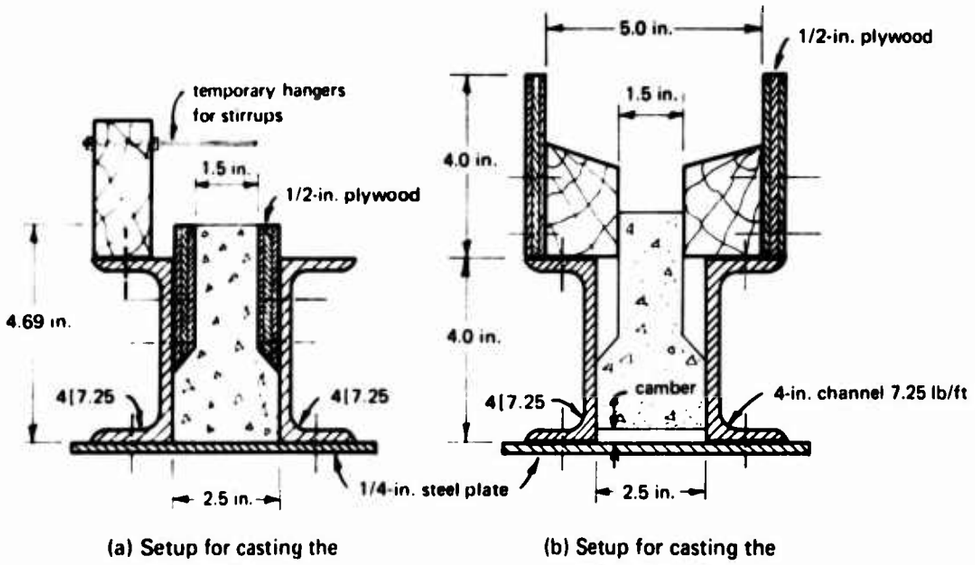

(a) Setup for casting the precast part.

(b) Setup for casting the cast-in-situ part.

Figure 5. Forms for casting the precast and the cast-in-situ parts of test beams.

or a rough surface using a wire brush. The relative roughness can be visualized by comparing the finish of the two interfaces shown in Figure 6. The top surfaces of all cast-in-situ beam parts and all control cylinders were troweled smooth.

After casting the precast beam part, wet burlap was used to cover the concrete surface. Experience indicated that it was best to leave the beam in the form for at least 2 days; otherwise, the beam would break during handling. After the form was stripped, the precast beam part was wrapped in wet burlap until the tests of the control cylinders indicated enough strength for prestressing. Within 24 hours after prestressing and grouting, the cast-in-situ beam part was cast on the top of the precast beam part. The same curing procedure for the precast beam part was followed for the composite beam. Approximately 2 days before testing, the test beam was left to dry in the laboratory air. In all cases, the treatment of the control cylinders was similar to that of the corresponding test beam. At the time of testing, the age of concrete for the precast and the cast-in-situ parts averaged 16 and 6 days, respectively.

Figure 6. Beams showing rough and smooth interfaces.

Prestressing. The various components used in the prestressing operation were:

1. A 30-ton center-hole hydraulic jack driven by a hand-operated hydraulic pump
2. A jacking frame
3. Three grips
4. Two sets of load cells and strain indicators
5. Shims of various thicknesses

The general layout for the prestressing operation together with the details at the jacking end are shown in Figure 7, and a photograph of a disassembled grip is shown in Figure 8.

At the beginning of the prestressing operation, grip no. 1 was loosened so that its gripping action would not take place at the initial stage of the tensioning. When the pump was operated, the travel of the ram was resisted by grip no. 2 at one end and grip no. 3 at the other end of the beam (Figure 7a). The thrust was transferred from the jack to grip no. 2 through a washer, load cell no. 1, the jacking frame, the test beam, to load cell no. 2, in that order. A 1/2-inch bearing plate embedded in the beam (Figure 7b) was used to distribute the thrust transmitted to the beam through the jacking frame. A similar plate was used at the unjacked end for the same purpose. The tensioning was temporarily stopped when the reading of the strain indicator corresponded to a thrust of about 10 kips. Grip no. 1 was then tightened until its gripping action started to take place. At this stage, no shims were used, that is, grip no. 1 was directly in contact with the bearing plate of the jacking beam end. The jack pressure was then released. As a result, load cell no. 1 indicated a zero thrust, that is, there was no tension in the part of the strand between grip no. 3 and grip no. 1. Load cell no. 2, however, indicated that the tension trapped in the strand between grip no. 1 and grip no. 2 was, on the average, 6.5 kips. The drop of the value of thrust from 10 kips to 6.5 kips, or the prestress loss, is due to anchorage take-up at grip no. 1.

The jack pressure was applied again causing a retensioning of the part of the strand between grip no. 1 and grip no. 3. When the thrust at load cell no. 1 exceeded about 6.5 kips, a gap started to form between grip no. 1 and the bearing plate at the jacking end of the test beam. The gap size increased with further increase in the jack pressure. A shim (or shims) in the form of a split washer was inserted in the gap. The jack pressure was released again causing the thrust at load cell no. 1 to drop back to zero and the thrust at load cell no. 2 to reduce in value. The reduction in the value of thrust at

load cell no. 2 was proportional to the clearance required for the insertion of the shim(s). The thickness of the shim(s) selected was such that the thrust indicated by load cell no. 2 after the final release of the jack pressure was as close as possible to a preselected value. The maximum value of thrust, which is that recorded just before the final release, was the jacking prestress force denoted by F_{sj} in Table 1. The initial prestress force, F_{si}, was that indicated by load cell no. 2 just after the final release. The effective prestress force, F_{se}, was recorded at the time the composite section was tested.

After the initial prestress force was recorded, the jack travel was decreased until it was possible to disassemble grip no. 3. Grips no. 1 and 2, shim(s), and load cell no. 2 remained attached to the beam until after testing.

Two control cylinders were tested in compression prior to the prestressing operation to determine whether the concrete had gained enough strength. During or immediately after prestressing, four more cylinder tests were performed to evaluate the compressive strength and splitting tensile strength of the concrete.

Grouting. On the same day of casting the cast-in-situ part of the test beam, the precast prestressed part was placed in a form (Figure 5b) with the interface in a horizontal plane. When the form was completely assembled, the longitudinal axis of the precast beam part was forced to lie in a vertical plane. In other words, any sway that resulted from the prestressing was eliminated. The induced stresses resulting from this alignment were considered negligible.

The grout conduit (Figure 7b) was a corrugated flexible metal tube with 3/4-inch and 1-1/8-inch inside and outside diameters, respectively. The main part of the grout conduit surrounded the steel strand throughout the beam length. Two 1/8-inch-diameter holes were drilled in the bearing plates, which were embedded at the beam ends, for proper positioning of the main conduit. At about 6 inches from each end of the beam, the grout conduit branched upward. One of the branches served as an inlet for the pumped grout (Figure 7b); the branch at the other end served as an outlet for the air that would be displaced by the grout.

The grout ingredients were thoroughly mixed by hand and then fed into a grout pump. The grout pump was essentially a steel container connected to an air-pressure outlet. When the air-pressure valve was opened, the grout was pumped through a hose into the inlet of the grout conduit. The pumping was continued until grout was forced out of the conduit branch at the other end of the beam.

After grouting, the cast-in-situ part of the beam was cast. The prestressing was not released even after the grout gained "full" strength.

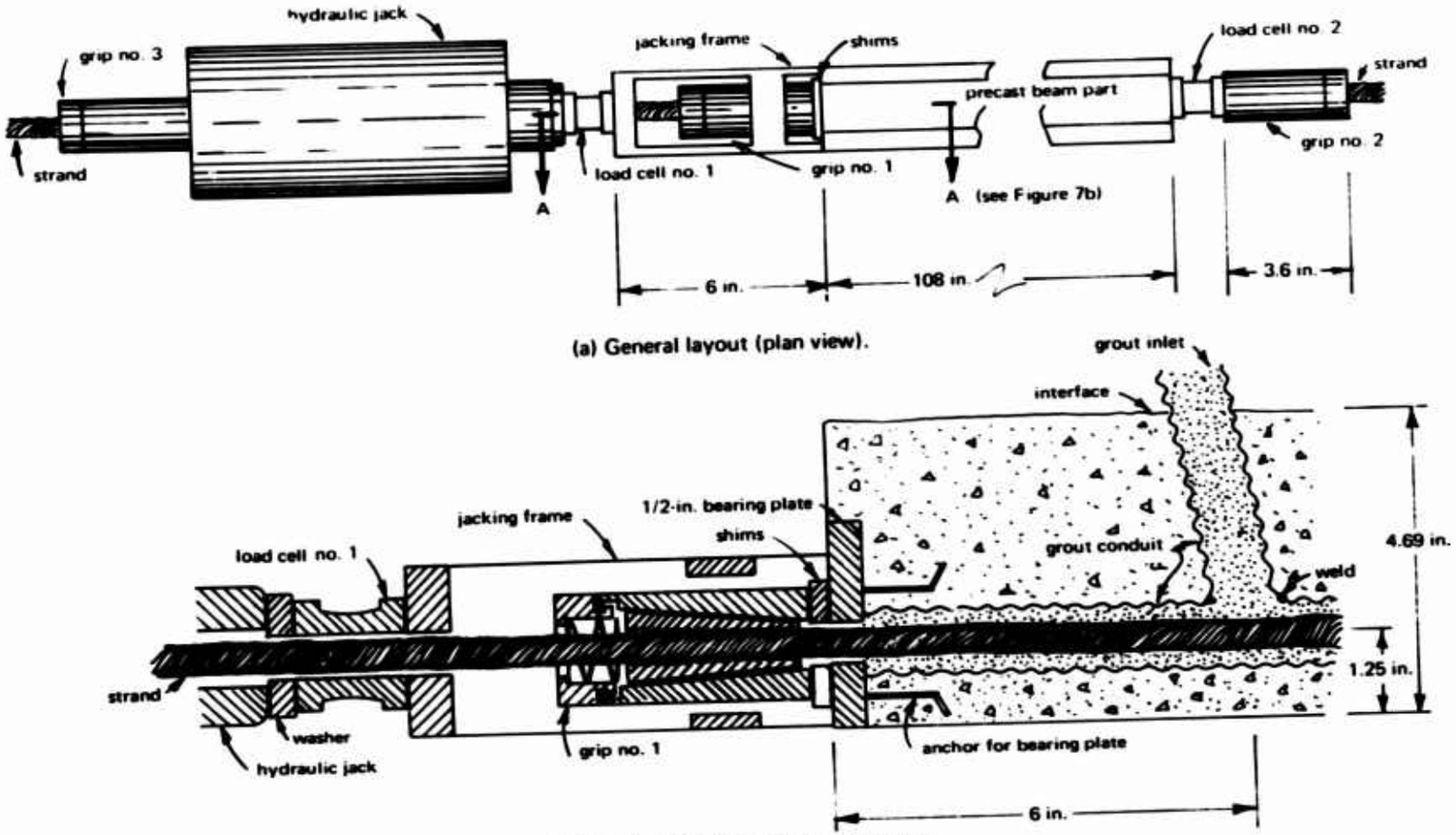

Figure 7. Setup and details for prestressing operation.

Figure 8. A disassembled grip.

Loading Equipment

The loading was applied by a 10-ton-capacity hydraulic jack driven by a hand-operated hydraulic pump. The jack (Figure 9) was connected to a rigid loading frame. The force provided by the jack was transmitted to the beam through a 10-ton-capacity load cell, a rocker, a bearing plate, a steel I-beam, and two sets of rockers and bearing plates, in that order. The load cell was connected to a strain indicator that measured the total applied load. Another strain indicator was connected to the load cell at the beam unjacked end for measuring the change in the prestressing force during the test. The steel I-beam distributed the jack load equally to the two loading points of the test beam.

Slip between the precast and the cast-in-situ parts of the beam was observed at three locations along the interface as shown in Figure 9. Dial gages graduated to 0.001 inch were used for measuring both the slip and the midspan deflection.

All control cylinders were tested in a 400,000 pound-capacity universal testing machine.

Test Procedure

The beam was aligned so that the load was applied symmetrically and so that no torsional moments should develop. The beam test continued for about 2 to 3 hours, and the failure load was reached in 20 to 30 increments.

The first eight increments of load were 500 pounds each. The magnitude of the load increments was then reduced to 250 pounds until the beam failed. Immediately after each load increment was applied, readings of slip and midspan deflection gages were recorded together with the strain reading for the load cell at the beam end. The beam was marked at the locations of newly developed cracks and/or the extensions of preexisting cracks. A second set of readings was recorded prior to the addition of a new load increment.

Twelve control cylinders were tested for each test beam to determine the compressive strength and the split-cylinder tensile strength for the two beam parts. The stressing rate for the six compression tests was 35 psi/sec; for the six splitting tensile tests it was 110 psi/min. These rates conformed with ASTM C 39-66 and ASTM C 496-66, respectively.

RESULTS AND DISCUSSION

Beam Behavior and Mode of Failure

Failure occurred along the interface for test beams with a reinforcement parameter, $r f_y$, of 176 psi or less. Beams S2.0 and R2.0, which had reinforcement parameters of 670 psi, developed some cracks along the interface prior to failure in flexure. Interface cracking dominated the crack pattern of the entire span of beam S2.0 but was limited to the constant-moment region (the region between the two loading points) of beam R2.0. The condition of roughness at the interface did not influence the behavior and mode of failure of companion beams failing along the interface. However, the failure loads were consistently higher for beams with a rough interface as compared with their companion beams with a smooth interface. Distinct behaviors and modes of failure were observed when the reinforcement parameter varied from 0 to 670 psi. In the following discussion, beams are grouped according to the value of the reinforcement parameter, $r f_y$.

Beams With an $r f_y$ of 0 and 73.5 psi. During the initial stages of loading, the beam's midspan deflection was proportional to the applied load up to about 80% of the load at first cracking. When the load reached about 5 kips, one or more flexural cracks opened within the constant-moment region. Additional load increments caused some of the existing cracks or newly developed cracks to extend above but not along the interface. At about 80% of the failure load, flexural cracks opened within one or both shear spans only several inches from a loading point. Such cracks extended towards the loading point and stopped underneath it. With a further increase in the load, the beam failed suddenly due to a separation along the interface. This separation extended from a point

near one of the beam reactions all the way to the beam midspan. Beam R0.0, shown in Figure 10, has a typical crack pattern after failure of beams with $r f_y \leq 73.5$ psi. Splitting along the interface took place between the reaction and the neighboring beam end only for beams with a smooth interface. Simultaneously with the interface splitting, a "relief crack" opened across the top flange about 5 inches from the support as shown in Figure 11. After failure, the load dropped to about 4.3 and 6.0 kips for beams with an $r f_y$ of 0 and 73.5 psi, respectively.

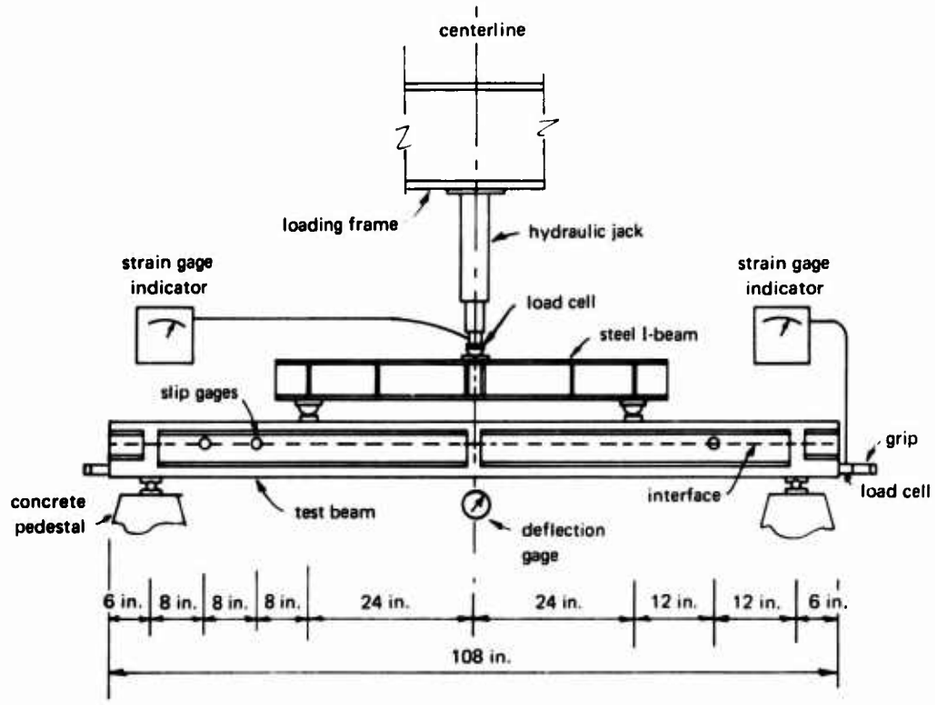

Figure 9. Test setup.

Prior to failure, there was no change in the value of the prestressing force at the beam end. This indicates that the grout strength was high enough for bonding. At failure, beams that showed a change in the prestressing force were those which failed at the unjacked end or where the load cell was provided. It is interesting to note that all beams with a rough interface failed at the unjacked end, while beams with a smooth interface failed at the jacking end.

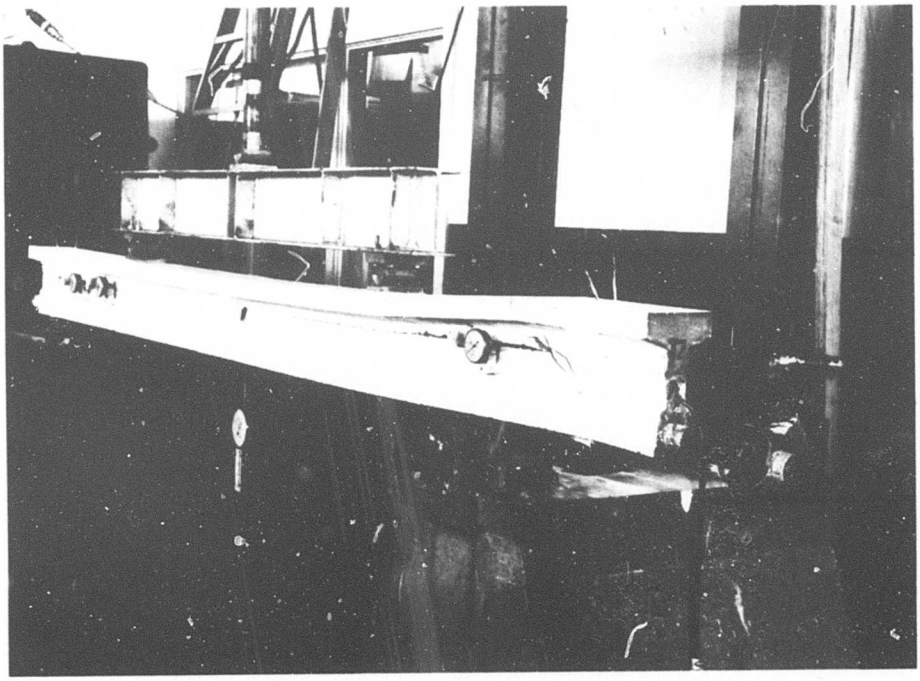

Figure 10. Typical failure of test beams with $r f_y \leq 73.5$ psi.

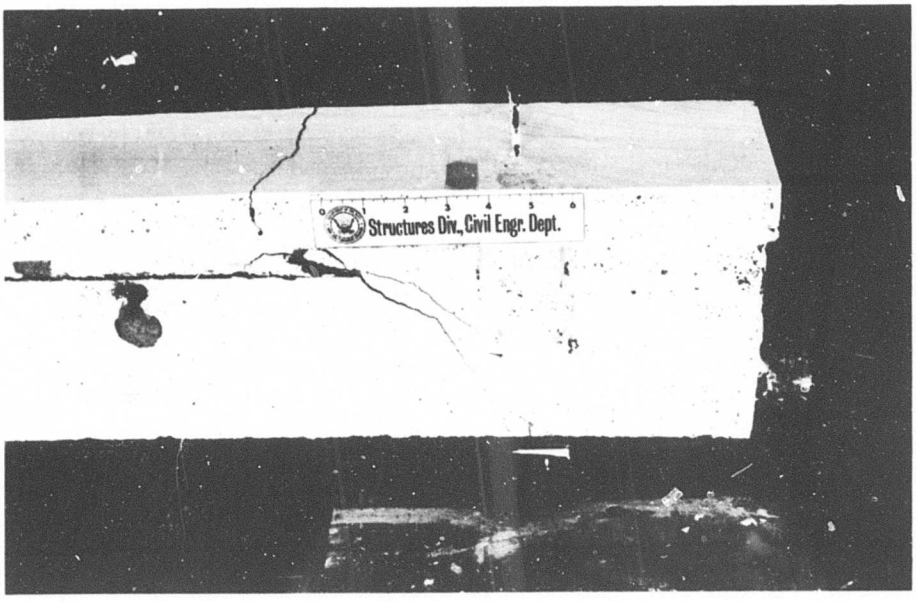

Figure 11. Cracking of top flange.

Beam S0.0 was the only beam in this group that developed visible cracking along the interface prior to failure; this occurred when the load was about 95% of the ultimate load. For all beams of this group, the maximum value of measured slip was limited to about 0.001 inch until failure. When failure occurred, however, the slip suddenly increased to about 1/4 inch.

Beams With an $r f_y$ of 176 psi. The two beams, S0.7 and R0.7, forming this group behaved similarly to the beams with smaller values of $r f_y$ in that: (1) before cracking, the midspan deflection was proportional to the applied load, (2) the first visible cracks were flexural cracks appearing within the constant-moment region, and (3) flexural cracks appearing within the shear span developed near a loading point and progressed towards it but stopped underneath it. Further loading did not cause sudden splitting as in the case of beams with $r f_y \leq 73.5$ psi. Instead, cracks became visible along the interface at both shear spans of the test beam; this was accompanied with a noticeable increase in the measured slip. After the appearance of interface cracking and with further loading, the beam deflected at a faster rate. As the load approached failure, spalling of the concrete cover took place at the stirrup locations at the interface within only one of the two shear spans. Also, the concrete showed signs of crushing in the neighborhood of the loading point at the end of the shear span showing greater distress. At this stage, a slight increase of load produced large deflection and slip, leading finally to failure. Figure 12 is a photograph of the jacking end of beam S0.7, where failure took place. Spalling of the concrete cover at the stirrup locations was not as severe at one face of the beam as it was at the other face. This raised the question whether the stirrups were symmetrically embedded in the beams. However, closer examination of the beams after failure showed that one or more stirrups were ruptured at *both* branches.

As for beams with smaller $r f_y$, there was no change in the prestressing force, measured at the beam unjacked end, prior to failure. At failure, beam R0.7, which failed at the unjacked end, showed an increase in the prestressing force of about 1 kip.

Beams With an $r f_y$ of 670 psi. This group consisted of the test beams S2.0 and R2.0. Both beams failed in flexure, but the patterns of crack formation for the two beams were different. In the early stages of loading, both beams behaved similarly to the beams with smaller values of $r f_y$. At higher loads, beam S2.0 behaved similarly to the beams with an $r f_y$ of 176 psi, until cracks were developed along the interface within the two shear spans. However, increasing the applied load did not increase the slip drastically and did not cause any spalling of the concrete cover at the stirrup locations. As the

load was further increased, cracks along the interface developed almost everywhere between the two reactions including the constant-moment region. Near the supports, the interface cracks branched diagonally downward and progressed towards the reactions. Within the constant-moment region, cracks were visible at several locations where the web meets the bottom flange.

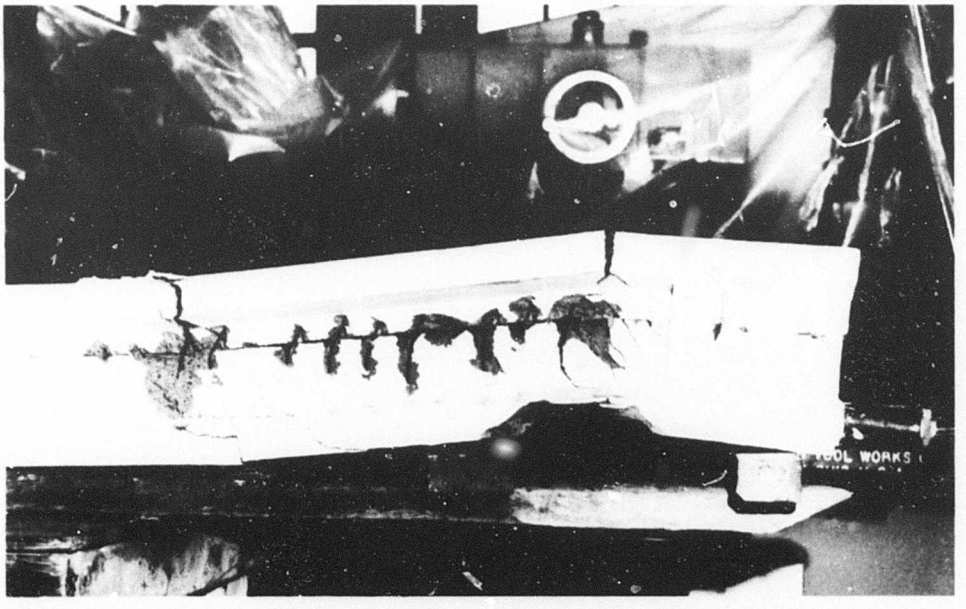

Figure 12. Severe cracking along the interface of test beams with $r f_y$ = 176 psi.

The load cell at the unjacked end of beam S2.0 showed an increase in the prestressing force when the applied load reached 11.25 kips. Additional load increments caused the top flange to develop a relief crack within the shear span at about 3 inches from the unjacked end. This caused a drop in the prestressing force of about 3 kips. Prior to beam failure, a similar relief crack opened close to the jacking end, and signs of concrete crushing appeared at the loading points.

Failure occurred by the crushing of concrete underneath a loading point as shown in Figure 13; this was accompanied by a separation along the interface between the two supports. At failure, the increase in the value of the prestressing force at the beam end was 7.5 kips.

Figure 13. Flexural failure of beam S2.0.

Among all the test beams, R2.0 was the only beam that did not develop, within the shear spans, visible splitting cracks along the interface or relief cracks at the top flange. The beam failed in flexure at a load slightly higher than the calculated flexural resistance. The maximum value of measured slip did not exceed 0.002 inch even after failure occurred.

Flexural cracks in beam R2.0 appeared first within the constant-moment region then within the shear spans near the loading points. When the load was increased, flexural cracks within the constant-moment region reached the interface and then extended down both sides along the interface. Flexural cracks within the shear spans turned towards the loading points and crossed the interface without traveling along it. Several diagonal cracks originated in the web within the shear spans but did not develop into interface cracking. Prior to failure, the constant-moment region was dominated by three types of cracks: (1) flexural cracks mostly within the precast beam element, (2) splitting cracks along the interface, and (3) cracks parallel to the longitudinal beam axis located at the junction of the web and the bottom flange. The flexural failure of the beam took place at the load point near the unjacked end with separation of the two beam parts at the interface within the constant-moment region (Figure 14).

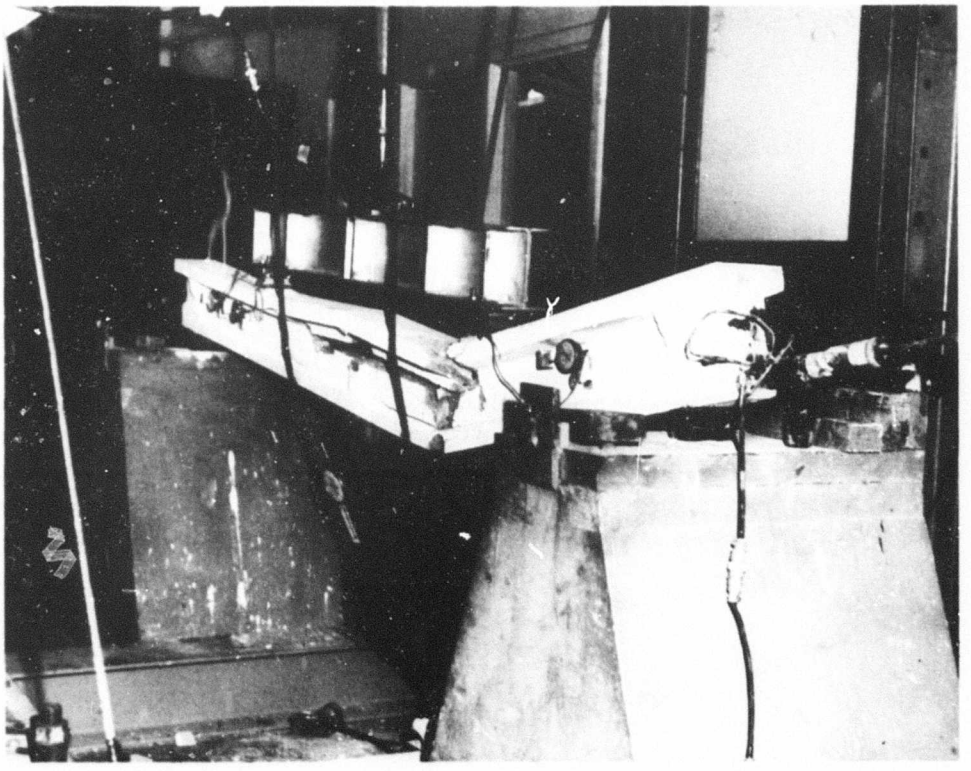

Figure 14. Flexural failure of beam R2.0.

Deviation From Condition for Split-Beam Prestressing

According to Reference 1, split-beam prestressing requires the interface to pass through the centroid of the composite section. This condition was one of the criteria that governed the design of the test beams. A check is, therefore, required to see whether this condition is still satisfied when the actual, rather than the nominal, section properties are the basis for the calculation. The likelihood of satisfying this condition precisely is remote; however, one can expect a narrow margin within which the test beams satisfy this condition of split-beam prestressing. In order to find such a margin, a yardstick is needed to determine a meaningful measure of the deviation from the condition that the interface must pass through the centroid. The measure adapted herein is the ratio of the horizontal shear stress at the interface to that at a plane parallel to the interface and passing through the centroid of the composite section. This ratio is equal to the ratio Q_i/Q_m, where Q_i and Q_m are the first moments of area (about the maximum principal axis of inertia) for the areas above the interface and above the plane through the centroid, respectively.

According to this definition, a split beam is a composite beam with the value of Q_i/Q_m being unity. The values of Q_i/Q_m for all the test beams are shown in Table 3. The deviation of the value of Q_i/Q_m from unity did not exceed 0.01 for any of the test beams. It can be said, therefore, that the test beams satisfied the split-beam prestressing requirement within the narrow margin of 0.01.

Calculated Stresses and Resistances

Utilizing the actual material characteristics and the geometry of the test beams, the properties of the beam sections were determined at the time of prestressing and at the time of testing and are tabulated in the Appendix. These properties were used to evaluate the normal and shear stresses, load at first flexural cracking, and the ultimate flexural resistance of the test beams. The elastic modulus for concrete was based on Section 8.3.1 of the ACI Code.[22]

Stresses Before and at Initiation of Flexural Cracking. The stress distribution patterns at the midspan of the test beams were determined for three stages of loading conditions, namely:

Stage A — Prestressing-steel stress equals the measured jacking stress f_{sj} (Table 1), considering the dead weight of the precast part to be the only applied load.

Stage B — Prestressing-steel stress equals the measured effective stress f_{se} (Table 1), considering the dead weight of the composite section to be the only applied load.

Stage C — Bottom-fiber concrete stress equals the concrete splitting strength (measured from control cylinder tests) with both the dead weight of the composite section and the externally applied load acting.

In order to perform the calculations systematically, the five cases presented in Table 4 were considered. Case 1 directly yields the stresses required to determine the stress distribution pattern for Stage A, shown in Figure 15. The stress distribution pattern for Stage B (Figure 15) was obtained by superpositioning the stresses from cases 2 and 3 (Table 4).

The value of the concrete strain, ϵ_{cse}, at the prestressing-steel level (when the prestressing-steel stress equals the effective stress) plays an important role in analyzing prestressed concrete beams. This strain, ϵ_{cse}, which was obtained directly from the corresponding stress of Stage B, was used in determining the stress pattern for Stage C as will be seen from the following discussion.

Table 3. Summary of Results

Beam Designation	Beam Data		Test Results				Shear Stresses[b]		Predicted Resistance		$\frac{P_c}{P_{cp}}$	$\frac{P_u}{P_{uf}}$	$\frac{w_u}{w_c}$	Failure Mode[c]
			Loads		Deflections									
	$\frac{Q_i}{Q_m}$	$\frac{Q_i}{lb'}$ (1/in.)	P_c[a] (kips)	P_u[b] (kips)	w_c[a] (in.)	w_u[b] (in.)	$\frac{VQ_i}{lb'}$ (psi)	$\frac{V}{b'd_s}$ (psi)	P_{cp}[a] (kips)	P_{uf}[b] (kips)				
S0.0	0.996	0.119	5.24	7.75	0.218	0.540	469	405	5.47	12.1	0.957	0.643	2.48	IJ
R0.0	0.994	0.120	5.25	9.25	0.196	0.795	565	490	5.14	11.7	1.02	0.791	4.06	IU
S0.3	0.993	0.118	4.80	7.62	0.245	0.770	458	397	5.31	12.4	0.903	0.616	3.14	IJ
R0.3	0.992	0.120	5.69	10.00	0.249	1.186	607	528	5.55	11.7	1.03	0.852	4.76	IU
S0.7	0.997	0.118	5.50	9.87	0.197	1.800	593	512	5.86	12.4	0.939	0.797	9.14	IJ
R0.7	0.995	0.119	3.50	11.17	0.129	1.310	672	581	4.35	12.2	0.805	0.913	10.16	IU
S2.0	0.994	0.116	5.50	13.25	0.222	2.557	779	674	6.08	13.0	0.904	1.02	11.52	FU
R2.0	0.995	0.116	5.50	14.50	0.183	2.100	852	736	6.79	12.9	0.810	1.12	11.48	FU

[a] At the initiation of flexural cracking.

[b] At ultimate load.

[c] IJ and IU denote failure along the Interface at the Jacking end and the Unjacked end, respectively; FU symbolizes Flexural failure underneath the loading point near the Unjacked end.

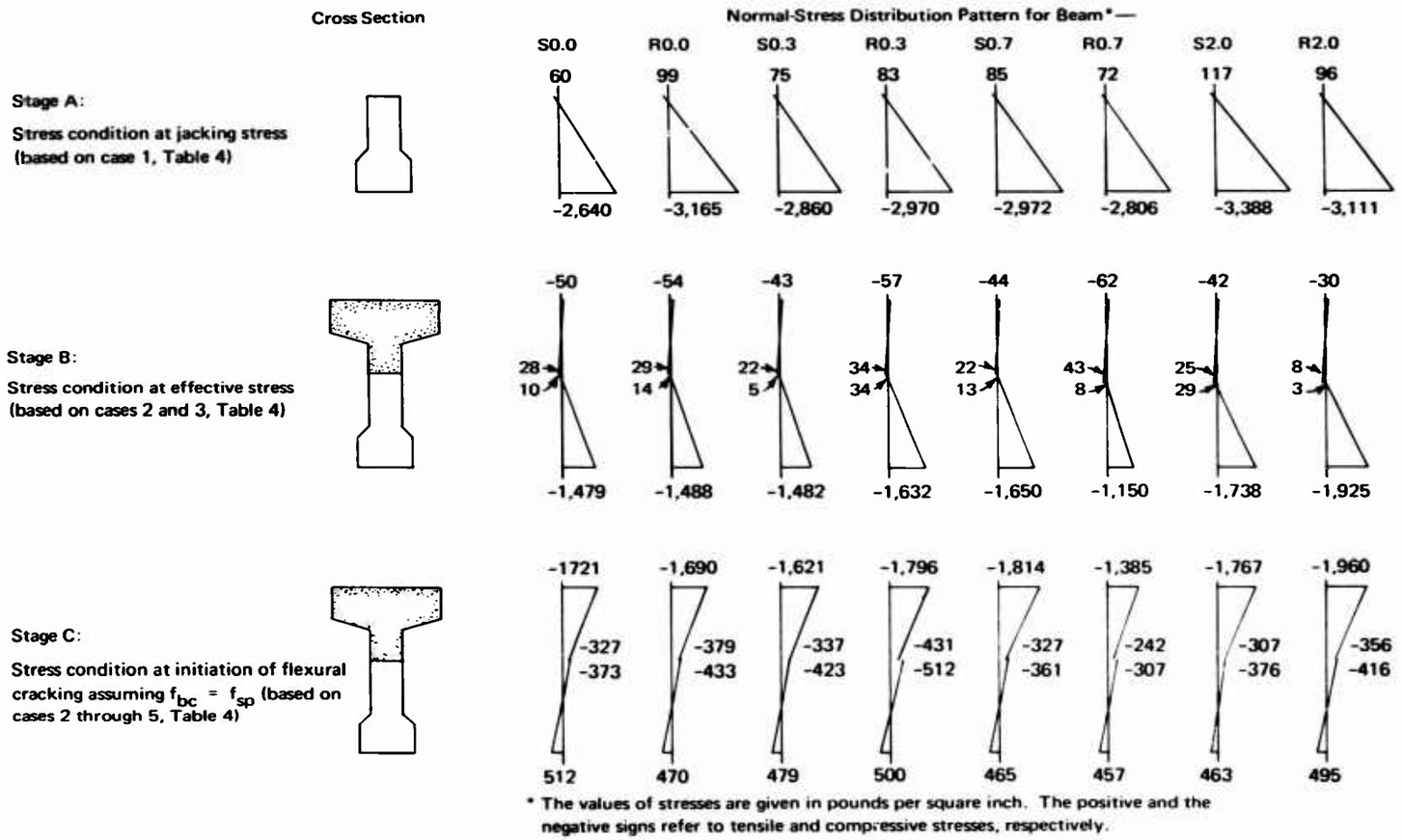

* The values of stresses are given in pounds per square inch. The positive and the negative signs refer to tensile and compressive stresses, respectively.

Figure 15. Normal-stress distribution patterns for the test beams.

Table 4. Basic Cases of Loading Considered for the Determination of Various Stress Patterns

Case No.	Forces		Section Considered	Effective Area
	External, **P** (kips)	Internal, F_s (kips)		
1	0	F_{sj}	precast part only	net
2	0	F_{si}	precast part only	gross transformed
3	0	$-F_{s\ell}$	composite section	gross transformed
4	0	-1	composite section	gross transformed
5	1	0	composite section	gross transformed

In order to determine the stress pattern for Stage C, one needs to evaluate the value of the externally applied load and the associated increase in the prestressing force that satisfies the following two conditions: (1) the bottom-fiber concrete stress equals the concrete splitting strength, and (2) the increase in the prestressing-steel strain above the value ϵ_{cse}. These two conditions can be written in terms of the stresses and strains obtained for cases 2 through 5 (Table 4) as below:

$$f_{b2} + f_{b3} + \alpha f_{b4} + \beta f_{b5} = |f_{sp}|$$

and

$$|\epsilon_{cse}| + \alpha|\epsilon_{cs4}| + \beta|\epsilon_{cs5}| = \frac{\alpha}{E_s A_s}$$

where A_s = area of prestressing steel

E_s = elastic modulus of prestressing steel = 29×10^6 psi

f_{bi} = bottom-fiber concrete stress from case i

f_{sp} = splitting concrete strength

i = subscript referring to cases 2, 3, 4, and 5 (Table 4)

α = increase in prestressing force at Stage C above that at Stage B

β = magnitude of the externally applied load, **P**, at Stage C

ϵ_{cse} = algebraic sum of concrete strains at the steel level from cases 2 and 3

ϵ_{csi} = concrete strain at the steel level for case i

These two simultaneous equations yielded the values of α and β that determined the stress pattern for Stage C (Figure 15). This was done by superpositioning the stresses obtained for case 2, case 3, α times the stresses for case 4, and β times the stresses for case 5.

It is to be emphasized that the value of β is the magnitude of the externally applied load at first cracking, P_{cp}, *based on the criterion that the flexural cracking is initiated when the concrete tensile stress reaches* f_{sp}. It is, therefore, interesting to compare this predicted cracking load, P_{cp}, with the load at the first observed flexural crack, P_c.

Values of P_c and P_{cp} are listed in Table 3 and are plotted in Figure 16. The ratio of measured to predicted load at first cracking, P_c/P_{cp}, ranged from about 0.8 to 1.0 (Table 3).

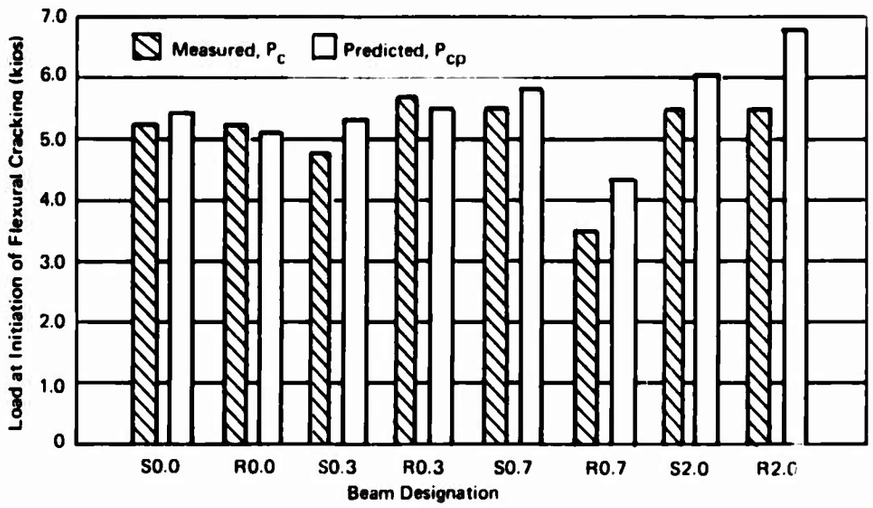

Figure 16. Measured and predicted loads at initiation of flexural cracking.

Stresses at Ultimate Load Versus Ultimate Strength. In order to decide whether a calculated stress at failure is the ultimate strength, the failure mode has to be recognized. One of the best approaches to identify the failure mode of a reinforced concrete member is to examine the crack propagation pattern. Another approach may be to see whether the predicted resistance, for a particular failure mode, was developed. The latter approach, however, depends heavily on the level of confidence in the assumptions made to predict the resistance. For the problem in hand, examination of the crack patterns leads to the conclusion that the test beams with $r f_y \leq 176$ psi failed in shear transfer while the two beams with $r f_y = 670$ psi failed in flexure. In order to check whether a similar conclusion could have been reached by comparing the failure load, P_u,

with the predicted flexural resistance, P_{uf}, (assuming full composite action), Figure 17 was constructed. Indeed, the ratio P_u/P_{uf} reached or exceeded unity for only the two beams with $r f_y$ = 670 psi. That is, increasing $r f_y$ to 670 psi caused the test beam to sustain loads as high as their predicted flexural capacity, and, therefore, failure in flexure is to be expected.

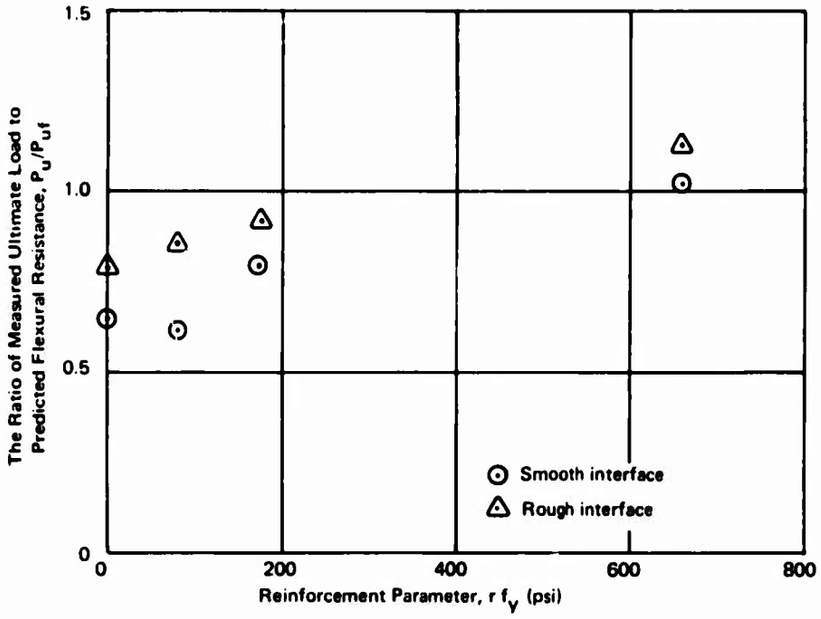

Figure 17. The ratio of measured ultimate load to predicted flexural resistance.

From Figure 17 (or Table 3) and the crack pattern at failure of the test beams discussed earlier, one concludes that horizontal shear stresses calculated at failure for beams with $r f_y \leq 176$ psi are the ultimate resistances. Also, one arrives at the obvious conclusion that $r f_y$ is a parameter that plays a major role in resistance to shear transfer. For test beams with $r f_y$ = 670 psi, the calculated values of horizontal shear stresses at failure constitute a lower bound of ultimate shear strength; that is, the calculated horizontal shear stresses are equal to or less than the ultimate values.

Deflection Response

As mentioned earlier, the load–midspan deflection response for all test beams was fairly linear in the early stages of loading. Figure 18 shows the deflection response for each set of companion beams, which differed mainly in the condition of roughness at the interface. Although consistent, the superiority of beams with rough interfaces was not too pronounced.

Comparing the response of beams with different reinforcement parameters, $r f_y$, one finds that both the "ductility" and the energy absorption capacity increased with the increase in $r f_y$.

The ratio of the midspan deflection at ultimate load, w_u, to that at first cracking, w_c, could be considered a measure of ductility. Table 3 lists the values of w_u/w_c for each test beam, and Figure 19 shows the graph of w_u/w_c as a function of $r f_y$. It is obvious that beams with $r f_y \geq 176$ psi were far superior in ductility to those with $r f_y \leq 73.5$ psi, regardless of the condition of roughness at the interface.

Load–Slip Diagrams

The graphs shown in Figure 20 give the relation between the maximum recorded value of slip and the magnitude of the load at which this slip was recorded. Due to the limited number of slip measurements, the maximum recorded slip constitutes a lower bound to the actual value of maximum slip. Therefore, the significance of the magnitudes of slip presented here is limited only to the comparison of the behavior of the test beams.

The load at which the value of slip became measurable does not seem to follow a certain trend or to have a consistent value. After initiation, the slip increased with the load at a rate of about 0.00015 in./kip of load. When the slip reached about 0.001 inch, failure of beams with $r f_y \leq 73.5$ psi occurred. For beams with $r f_y \geq 176$ psi, however, the slip continued to increase but at a much faster rate. The only exception was beam R2.0, for which the recorded slip was limited to 0.002 inch until flexure failure occurred.

The load–slip diagrams suggest that unless an appropriate amount of reinforcement is provided across the interface, failure could result from a sudden increase in slip or an eventual separation along the interface. It can also be concluded that the provision of reinforcement across the interface with a high $r f_y$ would minimize the slip and could lead to a more favorable mode of failure.

Horizontal Shear Stresses at the Interface

The horizontal shear stresses at ultimate load were evaluated using the standard formula $v = VQ_i/Ib'$. The assumptions made in obtaining this formula are seriously violated as soon as interface slip and cracking are developed. However, the use of the formula affords a common basis for comparison.[9, 11] The value of Q_i/Ib' (Table 3) was based on the gross transformed section at the middle of the shear span.

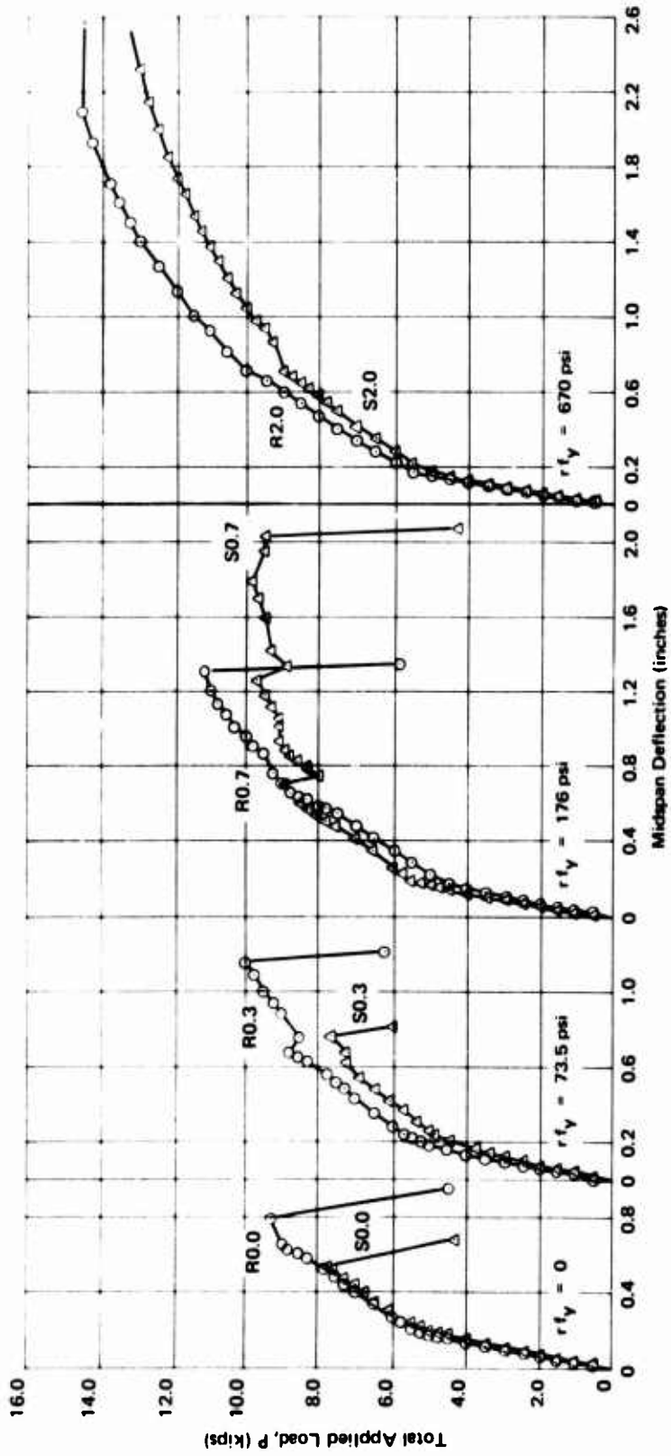

Figure 18. Load–deflection response of the test beams.

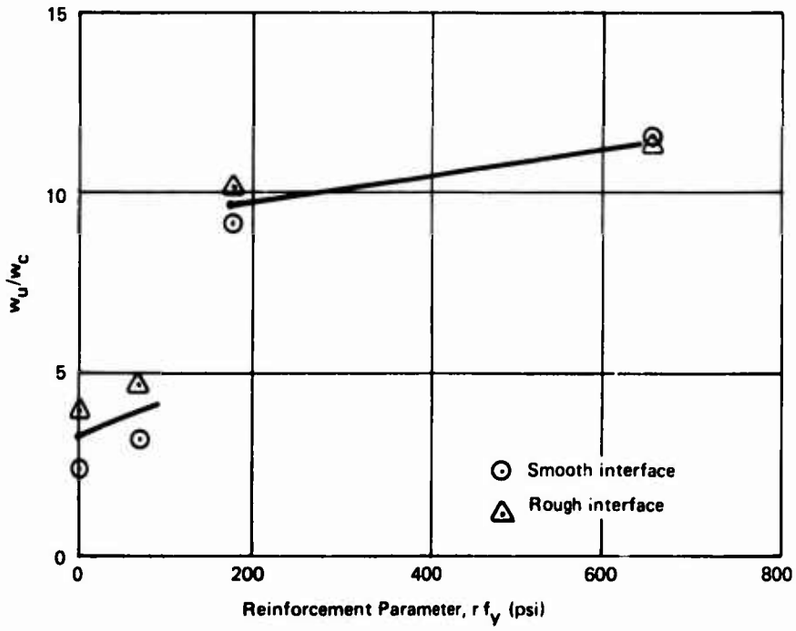

Figure 19. The ratio of midspan deflection at ultimate load to midspan deflection at first cracking.

As mentioned earlier, the ultimate horizontal shear strength for the test beams that failed along the interface ($r f_y \leq 176$ psi) is equal to the shear stress at ultimate load. The ultimate horizontal shear strength for the two test beams that failed in flexure is at least as high as the shear stress at ultimate load. Therefore, it is of interest to study the shear stress at ultimate load for *all* the test beams.

Figure 21 was constructed with each point representing the horizontal shear stress at ultimate load for two companion beams—one with a rough interface and the other with a smooth interface. The relationship for the ultimate horizontal shear strengths, Figure 21, may be approximated by

$$v_{ur} = 100 + v_{us}$$

where v_{ur} and v_{us} are the ultimate horizontal shear strength in pounds per square inch for rough and smooth interfaces, respectively. In other words, the ultimate horizontal shear strength for rough interfaces was approximately 100 psi higher than that for smooth interfaces when $r f_y$ varied between zero and 670 psi.

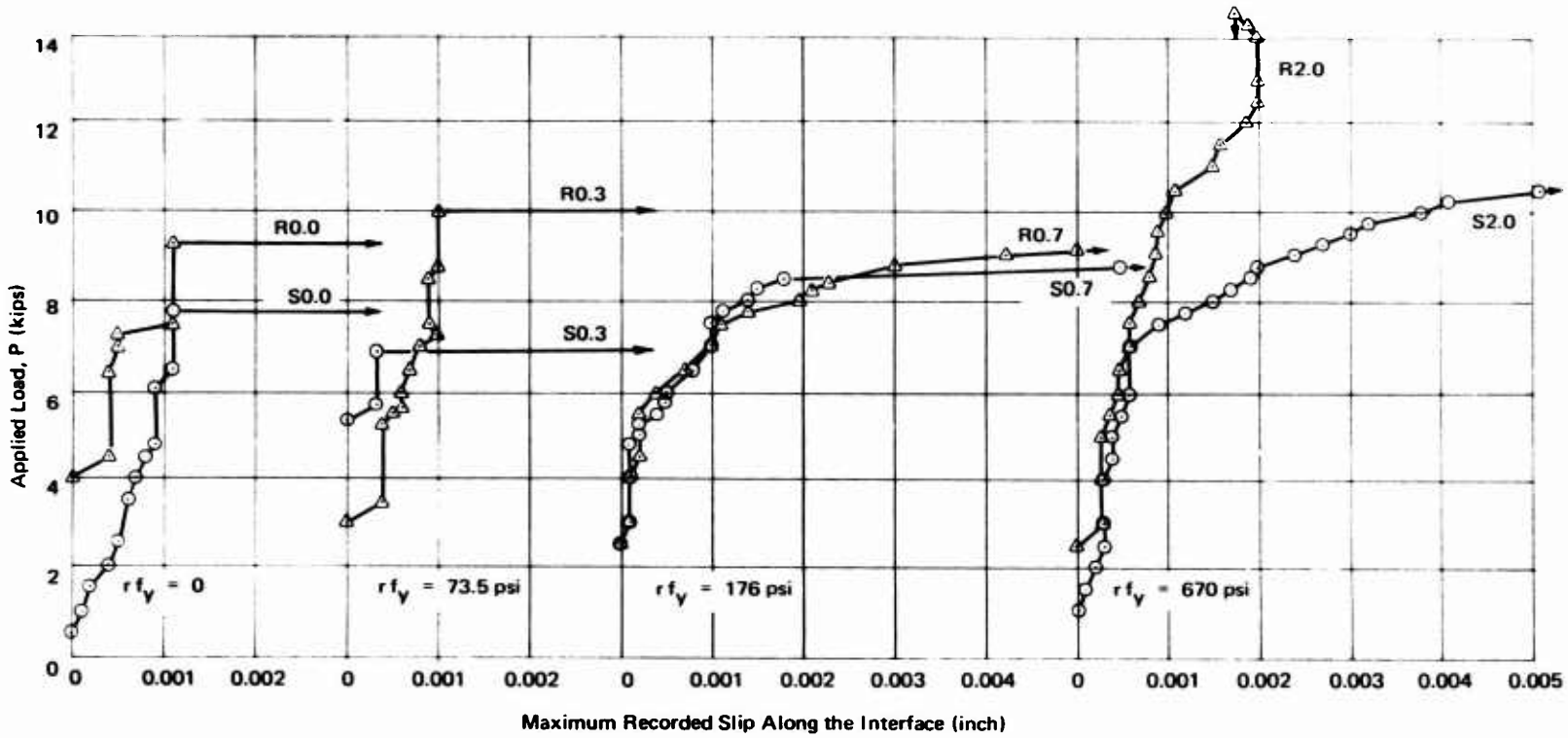

Figure 20. Load–slip diagrams.

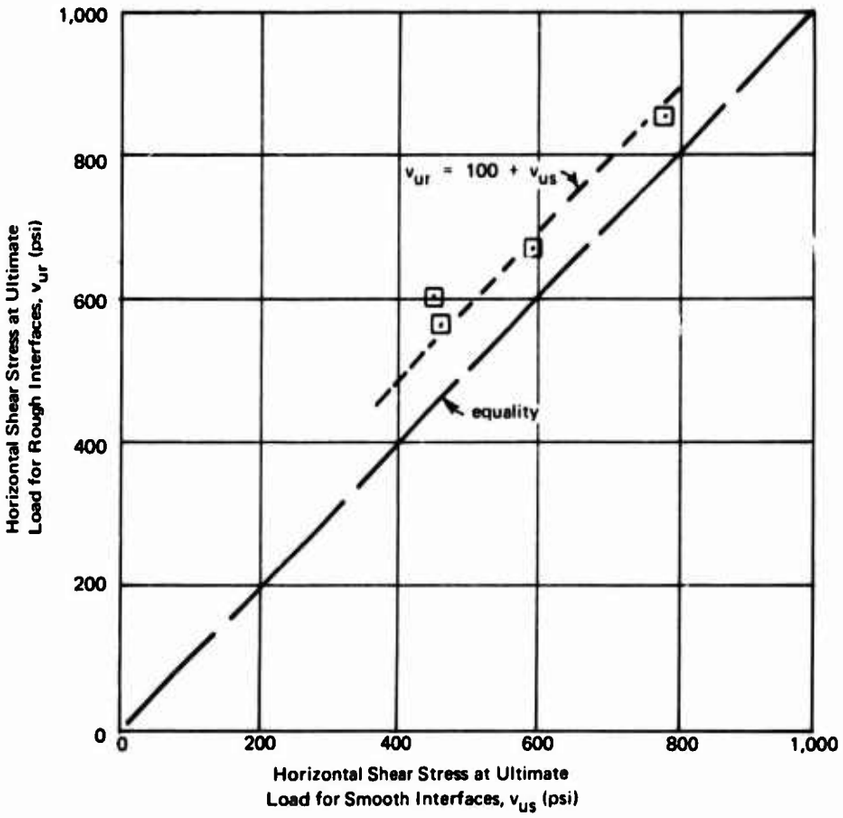

Figure 21. Comparison of horizontal shear stresses at ultimate load for smooth and rough interfaces.

Figure 22 shows the horizontal shear stresses at ultimate load for the test beams as a function of the reinforcement parameter $\mathbf{r f_y}$. This figure also shows graphs of functions of ultimate horizontal shear strength obtained from various sources.

The graphs obtained according to Reference 13 represent the equation of the shear friction hypothesis ($\mathbf{v_u = r f_v \tan \phi}$) with $\mathbf{\tan \phi} = 1.4$ for rough interfaces and $\mathbf{\tan \phi} = 0.7$ for smooth interfaces. Reference 13 recommended an upper limit of $\mathbf{r f_y} \leq 0.15 f_c'$, which was selected to terminate the curve for $\mathbf{\tan \phi} = 0.7$ at a value of $f_c' = 4{,}000$ psi. An upper limit of $\mathbf{v_u} \leq 800$ psi was given by Reference 12 and is shown in Figure 22 on the curve with $\mathbf{\tan \phi} = 1.4$. With such limitations, the shear friction hypothesis gave a conservative prediction of the shear resistance especially for the test beams with low values of $\mathbf{r f_y}$.

The graph shown in Figure 22 representing the recommendations of Reference 10 is based on the equation $v_u = 2{,}700/[(\mathbf{a/d}) + 5]$ with the shear-span-to-depth ratio, **a/d**, taken as 3.68, which is the average of the values of $\mathbf{a/d_s}$ listed in Table 1. Although this equation was intended only for rough-bonded interfaces, the stress data points for all beams failing along the interface fell well above the graph of the recommended expression.

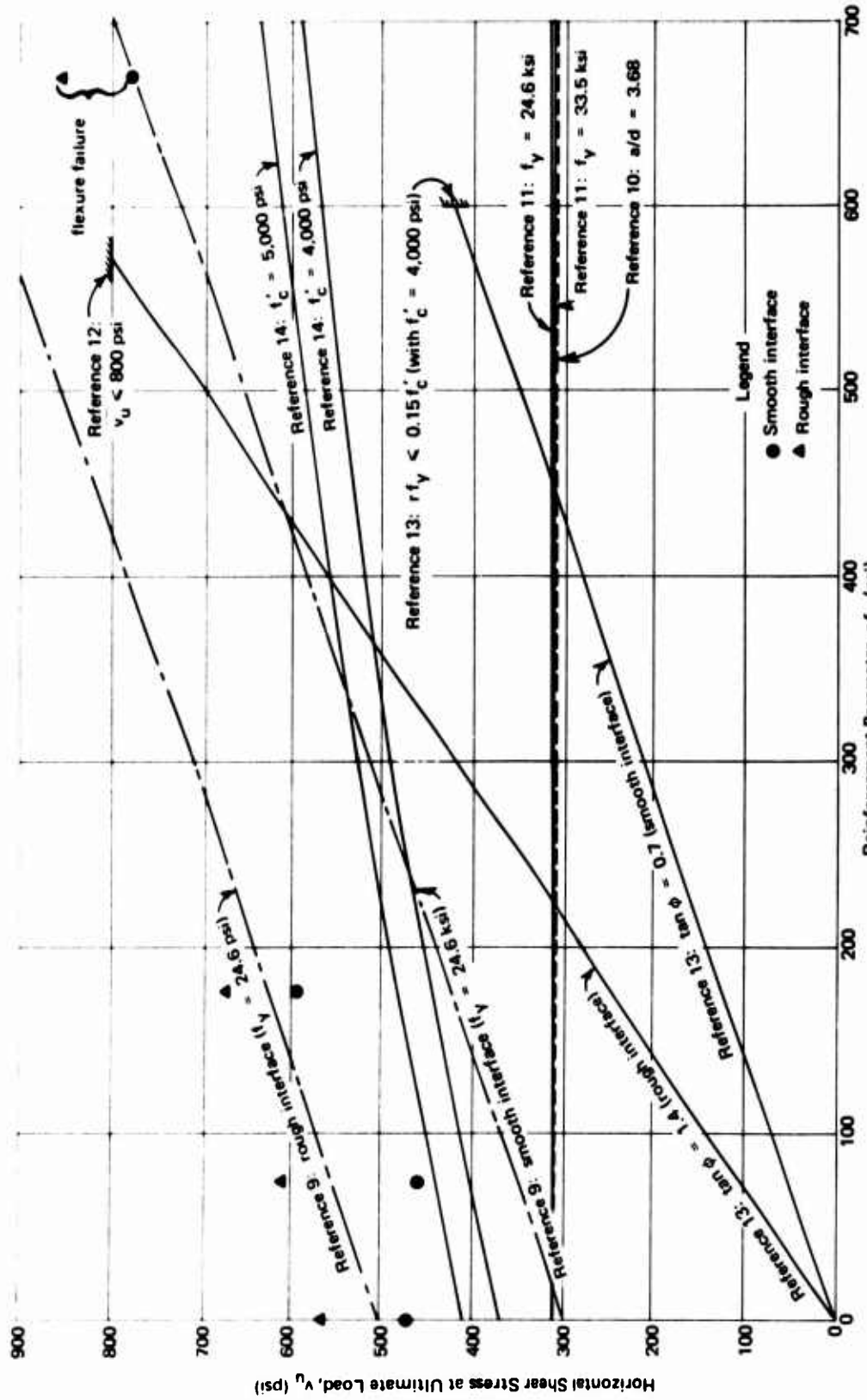

Figure 22. The relation between horizontal shear stress at failure and the reinforcement parameter.

Reference 11 suggests a linear relation between the ultimate horizontal shear strength, v_u, and the percent of reinforcement across the interface, r, which can be written in the form $v_u = a_1 + a_2 r$, where both a_1 and a_2 are functions of the shear-span-to-depth ratio, a/d. This relation does not take into account the yield point of the web steel, f_y. However, the equation could be rewritten in the form $v_u = a_1 + (a_2/f_y)(r f_y)$, which is suitable for producing the graphs shown in Figure 22 for Reference 11. The values of f_y = 33.5 and 24.6 ksi represent the yield point for the web steel across the interface for the test beams with $r f_y$ = 0 and 670 psi and $r f_y$ = 73.5 and 176 psi, respectively (Table 1). When a/d = 3.68 is taken as the average value for the test beams, the values of a_1 and a_2, according to Reference 11, become 311 and 217, respectively. Using these values, the recommended relation gives practically the same graph as that recommended by Reference 10, and, therefore, it is also conservative.

The recommendations given in Reference 9 could be written in the form $v_u = c + 17{,}500 r$, where r is the percent of web reinforcement across the interface, and c is to be taken as 300 psi for smooth interfaces and 500 psi for rough interfaces. When this relation was graphed in Figure 22, it gave a reasonable fit for the test data points of the beams that failed along the interface.

Reference 14 stated that the relation between the ultimate horizontal shear strength and the reinforcement parameter, $r f_y$, may be obtained using the concrete failure criterion suggested by Zia.[23] The graphs in Figure 22, according to this recommendation, bounded the test data points from below while maintaining the same general trend of variation of v_u with $r f_y$.

Figure 23 compares the test results to the values recommended in Section 17.5 of the ACI code.[22] The ordinate of each point is the value of the nominal horizontal shear stress at ultimate load, and the abscissa is the ACI code value for the beam under consideration. It is obvious that the code values are conservative especially for beams failing in horizontal shear.

FINDINGS AND CONCLUSIONS

1. The major effect of the condition of roughness at the interface of a split beam is on the ultimate horizontal shear resistance. The ultimate horizontal shear strength for the test beams with a rough interface was approximately 100 psi higher than that for companion beams with a smooth interface.

2. The reinforcement parameter across the interface, $r f_y$, has a significant effect on the beam behavior and the mode of failure. An increase in the value of $r f_y$ resulted in an increase in the "ductility" and the energy absorption

capacity of the test beam. The ultimate horizontal shear strength for beams with $\rho f_y = 0$ was in excess of 400 psi and increased at the rate of about 60 psi per 100 psi increase in ρf_y.

3. For values of the horizontal shear stress below 400 psi, the behavior of all beams was essentially the same, and the maximum value of the recorded slip was below 0.001 inch. When the maximum recorded slip reached about 0.001 inch, test beams with $\rho f_y \leq 73.5$ psi failed along the interface, while the test beams with $\rho f_y = 176$ psi offered more resistance but the slip increased at a much faster rate.

4. The ratio between the load measured at the initiation of flexural cracking and that predicted assuming full composite action ranged from 0.8 to unity.

5. In spite of the development of slip at the interface, the two beams which failed in flexure resisted loads as high as the predicted ultimate loads that were based on full composite action.

6. The ultimate horizontal shear strengths determined from the tests were much higher than those recommended by the ACI code.[22]

DESIGN RECOMMENDATION

The interface of a split beam is subjected to the highest value of horizontal shear stress in the composite section. Accordingly, special attention should be given to design against horizontal shear failure along the interface. Chapter 17 of the ACI Building Code Requirement[22] is recommended for safe prediction of the ultimate horizontal shear strength of a split beam.

ACKNOWLEDGMENTS

Mr. Lawrence Kahn supervised the fabrication of the test fixtures and assisted in the early stages of the testing. Mr. William Keenan provided helpful comments during the planning of the test program.

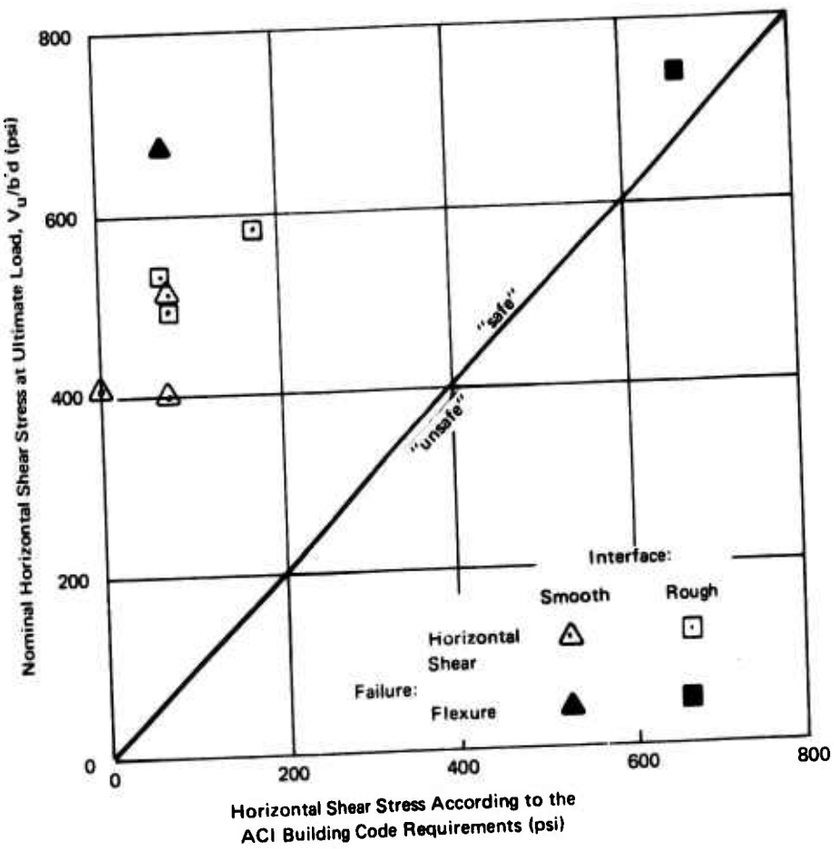

Figure 23. Comparison of observed and recommended horizontal shear stresses.

Appendix

PROPERTIES OF THE BEAM SECTIONS

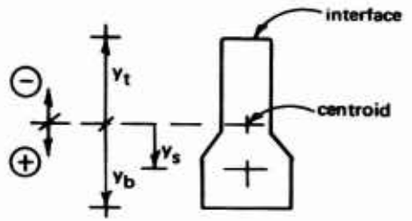

Table A-1. Properties of Precast Sections

Beam Designation	E_{pp} (psi x 10^6)	Properties of Precast Section[a] at—											
		Jacking Stress						Initial Stress					
		y_b (in.)	y_s (in.)	y_t (in.)	A (in.^{2})	I (in.^{4})	r_g^2 (in.^{2})	y_b (in.)	y_s (in.)	y_t (in.)	A (in.^{2})	I (in.^{4})	r_g^2 (in.^{2})
S0.0	3.65	2.16	0.91	-2.53	7.79	15.56	2.00	1.99	0.74	-2.70	9.54	16.83	1.76
R0.0	3.53	2.16	0.91	-2.53	7.79	15.56	2.00	1.99	0.74	-2.70	9.57	16.84	1.76
S0.3	3.34	2.16	0.91	-2.53	7.79	15.56	2.00	1.98	0.73	-2.71	9.62	16.87	1.75
R0.3	3.28	2.16	0.91	-2.53	7.79	15.56	2.00	1.98	0.73	-2.71	9.64	16.88	1.75
S0.7	3.63	2.16	0.91	-2.53	7.79	15.56	2.00	1.99	0.74	-2.70	9.55	16.83	1.76
R0.7	3.57	2.16	0.91	-2.53	7.79	15.56	2.00	1.99	0.74	-2.70	9.56	16.84	1.76
S2.0	4.00	2.16	0.91	-2.53	7.79	15.56	2.00	2.00	0.75	-2.69	9.47	16.78	1.77
R2.0	3.92	2.16	0.91	-2.53	7.79	15.56	2.00	1.99	0.74	-2.70	9.48	16.79	1.77

[a] Average section for the entire span.

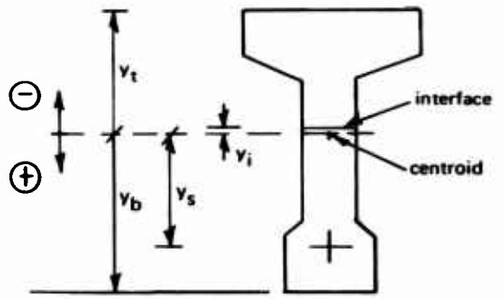

Table A-2. Properties of Composite Sections

Beam Designation	E_{ct} (psi x 10^6)	E_{pt} (psi x 10^6)	Properties of Composite Section[a] at—																	
			Midspan									Middle of Shear Span								
			y_b (in.)	y_s (in.)	y_i (in.)	y_t (in.)	A ($in.^2$)	I ($in.^4$)	r_g^2 ($in.^2$)	Q_i ($in.^3$)	Q_m ($in.^3$)	y_b (in.)	y_s (in.)	y_i (in.)	y_t (in.)	A ($in.^2$)	I ($in.^4$)	r_g^2 ($in.^2$)	Q_i ($in.^3$)	Q_m ($in.^3$)
S0.0	3.52	3.80	4.21	2.96	-0.49	-3.30	19.07	114.3	6.00	21.04	21.22	4.34	3.09	-0.35	-3.41	19.42	125.2	6.45	22.31	22.41
R0.0	3.53	3.86	4.09	2.84	-0.60	-3.22	18.67	105.8	5.66	19.35	20.20	4.28	3.03	-0.42	-3.38	19.15	120.1	6.27	21.66	21.79
S0.3	3.45	4.10	4.13	2.88	-0.56	-3.41	18.18	110.6	6.08	20.14	20.38	4.25	3.00	-0.44	-3.52	18.47	120.2	6.51	21.27	21.41
R0.3	3.33	3.91	4.02	2.77	-0.67	-3.29	18.05	102.4	5.67	19.21	19.54	4.20	2.95	-0.49	-3.46	18.50	116.6	6.31	20.94	21.12
S0.7	3.78	4.05	4.26	3.01	-0.44	-3.31	19.19	116.9	6.09	21.36	21.50	4.37	3.12	-0.32	-3.41	19.50	126.6	6.49	22.48	22.56
R0.7	3.64	4.03	4.19	2.94	-0.50	-3.31	18.79	112.7	6.00	20.72	20.91	4.32	3.07	-0.37	-3.43	19.13	123.4	6.45	21.98	22.08
S2.0	3.58	4.37	4.22	2.97	-0.47	-3.53	18.18	117.6	6.47	20.84	21.01	4.29	3.04	-0.41	-3.60	18.34	123.1	6.71	21.47	21.59
R2.0	3.53	4.19	4.24	2.99	-0.45	-3.51	18.45	119.3	6.47	21.17	21.32	4.31	3.06	-0.38	-3.57	18.61	124.9	6.71	21.80	21.91

[a] At the time of test.

REFERENCES

1. A. Amirikian. "Split-beam prestressing," Navy Civil Engineer, vol. 4, no. 11, Nov. 1963, pp. 35-39.

2. J. O. Bryson, L. F. Skoda and D. Watstein. "Flexural behavior of prestressed split-beam composite concrete sections," Prestressed Concrete Institute, Journal, vol. 10, no. 3, June 1965, pp. 77-91.

3. S. Revesz. "Behavior of composite T-beams with prestressed and unprestressed reinforcement," American Concrete Institute, Proceedings, vol. 49 (Journal, vol. 24, no. 6, Feb.) 1953, pp. 585-592.

4. R. H. Evans and A. S. Parker. "Behavior of prestressed concrete composite beams," American Concrete Institute, Proceedings, vol. 51 (Journal, vol. 26, no. 9, May) 1955, pp. 861-878.

5. A. R. Anderson. "Composite designs in precast and cast-in-place concrete," Progressive Architecture, vol. 41, no. 9, Sept. 1960, pp. 172-179.

6. B. Grossfield and C. Birnstiel. "Tests of T-beams with precast webs and cast-in-place flanges," American Concrete Institute, Journal, Proceedings, vol. 59, no. 6, June 1962, pp. 843-851.

7. W. E. Dean and A. M. Ozell. "No shear keys are needed here," Engineering News-Record, vol. 156, no. 23, June 7, 1956, pp. 61-62, 64.

8. W. E. Dean. "Beam test shows need for web steel," Engineering News-Record, vol. 157, no. 25, Dec. 20, 1956, pp. 36-37.

9. N. W. Hanson. "Precast-prestressed concrete bridges, pt. 2—Horizontal shear connections," Portland Cement Association Research and Development Laboratories, Journal, vol. 2, no. 2, May 1960, pp. 38-58; PCA Development Bulletin D35.

10. A. H. Mattock and P. H. Kaar. "Precast-prestressed concrete bridges, pt. 4—Shear tests of continuous girders," Portland Cement Association Research and Development Laboratories, Journal, vol. 3, no. 1, Jan. 1961, pp. 19-46; PCA Development Bulletin D45.

11. J. C. Saemann and G. W. Washa. "Horizontal shear connections between precast beams and cast-in-place slabs," American Concrete Institute, Journal, Proceedings, vol. 61, no. 11, Nov. 1964, pp. 1383-1409.

12. P. W. Birkeland and H. W. Birkeland. "Connections in precast concrete construction," American Concrete Institute, Journal, Proceedings, vol. 63, no. 3, Mar. 1966, pp. 345-368.

13. R. F. Mast. "Auxiliary reinforcement in concrete connections," American Society of Civil Engineers, Proceedings, Journal of the Structural Division, vol. 94, no. ST6, June 1968, pp. 1485-1504.

14. J. A. Hofbeck, I. O. Ibrahim and A. H. Mattock. "Shear transfer in reinforced concrete," American Concrete Institute, Journal, Proceedings, vol. 66, no. 2, Feb. 1969, pp. 119-128.

15. R. H. Evans and H. W. Chung. "Horizontal shear failure of prestressed composite T-beams with cast-in-situ lightweight concrete deck," Concrete, vol. 3, no. 4, Apr. 1969, pp. 124-126.

16. J. W. Hall and R. F. Mast. Discussion of "Horizontal shear connections between precast beams and cast-in-place slabs," by J. C. Saemann and G. W. Washa. American Concrete Institute, Journal, Proceedings, vol. 61, 1964, pp. 1807-1810. (Published in vol. 62, no. 6, pt. 2, June 1965)

17. J. C. Saemann and G. W. Washa. Closure of "Horizontal shear connections between precast beams and cast-in-place slabs," American Concrete Institute, Journal, Proceedings, vol. 61, 1964, p. 1810. (Published in vol. 62, no. 6, pt. 2, June 1965)

18. N. M. Hawkins. Discussion of "Auxiliary reinforcement in concrete connections," by R. F. Mast. American Society of Civil Engineers, Proceedings, Journal of the Structural Division, vol. 95, no. ST3, Mar. 1969, pp. 508-512.

19. S. B. Nosseir. Discussion of "Shear transfer in reinforced concrete," by J. A. Hofbeck, I. O. Ibrahim and A. H. Mattock. American Concrete Institute, Journal, Proceedings, vol. 66, no. 8, Aug. 1969, pp. 678-680.

20. J. A. Hofbeck, I. O. Ibrahim and A. H. Mattock. Closure of "Shear transfer in reinforced concrete," American Concrete Institute, Journal, Proceedings, vol. 66, no. 8, Aug. 1969, p. 680.

21. Naval Civil Engineering Laboratory. Technical Report R-564: Mix design for small-scale models of concrete structures, by D. S. Fuss. Port Hueneme, Calif., Feb. 1968. (AD 664956)

22. American Concrete Institute. Committee 318. "Proposed revision of ACI 318-63: Building code requirements for reinforced concrete," American Concrete Institute, Journal, Proceedings, vol. 67, no. 2, Feb. 1970, pp. 77-184.

23. P. Zia. "Torsional strength of prestressed concrete members," American Concrete Institute, Proceedings, vol. 57 (Journal, vol. 32, no. 10, Apr.) 1961, pp. 1337-1359.

LIST OF SYMBOLS

A	Area of beam cross section (in.^{2})
A_s	Area of prestressing steel (in.^{2})
A_v	Total area of web reinforcement across the interface (in.^{2})
A_{v1}	Total area of web reinforcement (in.^{2})
a	Shear span (in.)
a_1, a_2	Functions of the shear-span-to-depth ratio, a/d
b	Width of top flange (in.)
b'	Width of web (in.)
c	Constant; 300 psi for smooth interfaces, 500 psi for rough interfaces
D	Diameter (in.)
d	Distance from the extreme compression fiber to the centroid of the prestressing steel (in.)
d_c	Distance from the extreme compression fiber to the centroid of the prestressing steel at the beam midspan (in.)
d_s	Distance from the extreme compression fiber to the centroid of the prestressing steel at the middle of the shear span (in.)
E_{ct}	Elastic modulus of the cast-in-situ concrete at the time of testing (psi)
E_{pp}	Elastic modulus of the precast concrete at the time of prestressing (psi)
E_{pt}	Elastic modulus of the precast concrete at the time of testing (psi)
E_s	Elastic modulus of the prestressing steel (psi)
F_s	Measured prestressing force (kips)
F_{se}	Effective force of prestressing measured at the time of testing the composite beam (kips)
F_{si}	Initial force of prestressing measured immediately after the final release (kips)
F_{sj}	Maximum jacking force of prestressing measured before the final release (kips)
$F_{s\ell}$	Loss in prestressing force from the time immediately after the final release to the time of testing the composite beam ($=F_{si}-F_{se}$) (kips)
f_{bc}	Bottom-fiber concrete stress at the initiation of flexural cracking (psi)
f_{bi}	Bottom-fiber concrete stress for case i (psi)
f'_c	Compressive strength of standard concrete cylinder (psi)
f_{se}	Effective steel stress ($=F_{se}/A_s$) (ksi)
f_{si}	Initial steel stress ($=F_{si}/A_s$) (ksi)
f_{sj}	Maximum jacking steel stress ($=F_{sj}/A_s$) (ksi)
f_{sp}	Concrete tensile strength measured from split-cylinder test (psi)
f_y	Yield point of the web reinforcement (ksi)
I	Moment of inertia (in.^{4})
i	Subscript referring to cases 2, 3, 4, and 5 discussed in the text
ℓ_e	Distance from beam end to first stirrup (in.)
ℓ_s	Length within which stirrups are provided (in.)
P	Total of the two equal loads externally applied at the quarter points (kips)
P_c	Measured load at the initiation of flexural cracking (kips)

BLANK PAGE

Unclassified

Security Classification

DOCUMENT CONTROL DATA - R & D

Security classification of title, body of abstract and indexing annotation must be entered when the overall report is classified)

1. ORIGINATING ACTIVITY (Corporate author)

Naval Civil Engineering Laboratory
Port Hueneme, California 93041

2a. REPORT SECURITY CLASSIFICATION

Unclassified

2b. GROUP

3. REPORT TITLE

ULTIMATE HORIZONTAL SHEAR STRENGTH OF PRESTRESSED SPLIT BEAMS

4. DESCRIPTIVE NOTES (Type of report and inclusive dates)

Not final; March 1968–September 1969

5. AUTHOR(S) (First name, middle initial, last name)

S. B. Nosseir and R. N. Murtha

6. REPORT DATE	7a. TOTAL NO OF PAGES	7b. NO OF REFS
January 1971	43	23

8a. CONTRACT OR GRANT NO.	9a. ORIGINATOR'S REPORT NUMBER(S)
b. PROJECT NO YF 38.534.001.01.009	R-707
c.	9b. OTHER REPORT NO(S) (Any other numbers that may be assigned this report)
d.	

10. DISTRIBUTION STATEMENT

This document has been approved for public release and sale; its distribution is unlimited.

11. SUPPLEMENTARY NOTES	12. SPONSORING MILITARY ACTIVITY
	Naval Facilities Engineering Command Washington, D. C. 20390

13. ABSTRACT

This report deals with the horizontal shear resistance and behavior of prestressed concrete composite beams when the interface is selected to pass through the centroid of the composite section. Composite beams proportioned in this manner are referred to as prestressed split beams. A total of eight simply supported split beams were statically tested with the major variables being interface roughness and reinforcement parameter $r f_y$. (r and f_y are the percent and yield point of the web reinforcement across the interface.) All test beams were posttensioned and grouted and had the same nominal dimensions. Beams with rough interfaces showed an increase in the ultimate horizontal shear strength of about 100 psi over that of "duplicate" beams with smooth interfaces. The ductility and the energy absorption capacity increased with $r f_y$. The ultimate horizontal shear strength for beams with $r f_y = 0$ was in excess of 400 psi and increased at the rate of about 60 psi per 100 psi increase in $r f_y$. The two beams with the highest value of $r f_y$ failed in flexure. In spite of developing slip at the interface, these two beams developed the calculated flexural resistance based on full composite action. The horizontal shear resistance of the test beams failing in horizontal shear was much higher than the computed values based on the ACI code.

DD FORM 1 NOV 68 1473 (PAGE 1)

S/N 0101-807-6801

Unclassified

Security Classification

KEY WORDS	LINK A		LINK B		LINK C	
	ROLE	WT	ROLE	WT	ROLE	WT
Shear transfer (concrete-to-concrete)						
Composite beams						
Split beam prestressing						
Slippage						
Horizontal shear stress						